Analyst

PAPER

Chitosan–gold nanocomposite and its functionalized paper strips for reversible visual sensing and removal of trace Hg^{2+} in practice

Cite this: DOI: 10.1039/c8an01707g

Lei Hu, Baohui Zhu, Li Zhang, Hua Yuan, Qi Zhao and Zhengquan Yan *

To eliminate mercury contamination in aqueous environment, chitosan–gold nanocomposite and its functionalized paper strips were designed and developed for visual sensing and removal of trace Hg^{2+}. By simply immersing a common filter paper into the resultant composite dispersion, gold nanochromophores could be well dispersed with minor aggregation by virtue of the dual supporting roles of the chitosan and the filter paper. Under optimized conditions, the colour of both the chitosan–gold nanocomposite and its functionalized paper strips could change from dark red to yellow upon addition of Hg^{2+}, with a detection limit of 3.2×10^{-9} mol L^{-1} and 5.0×10^{-8} mol L^{-1}, respectively. Importantly, the chitosan–gold nanocomposite was non-toxic and could be utilized repeatedly for sensing trace Hg^{2+} in both environmental aqueous solutions and some fruit or vegetable juice samples, with satisfactory results. Furthermore, using the resulting functionalized filter-paper, more than 93.5% Hg^{2+} in aqueous solution with an initial concentration as high as 1.0×10^{-5} mol L^{-1} could be enriched and separated by a simple filtration process. The proposed operating mechanism is based on the reversible gold amalgam formation between the gold nanoparticles and Hg^{2+}. This study will be the first report for paper-based sensing to visually detect, enrich and remove Hg^{2+} with minimal secondary pollution.

Received 4th September 2018,
Accepted 31st October 2018

DOI: 10.1039/c8an01707g

rsc.li/analyst

1. Introduction

Accompanying the rapid development of modern industry, particularly the modern mining and electronic industries, various heavy metals have been unscrupulously released into the natural environment, and the resultant contamination is becoming increasingly severe.[1–12] Among all the heavy metal pollutants, Hg^{2+} is one of the most dangerous for human beings owing to its special affinity to the S element in proteins and enzymes.[13–15] Exposure to Hg^{2+} even at low levels could cause diseases in the brain, kidney, and central nervous system.[16–19] Furthermore, Hg^{2+} is non-biodegradable and accumulates in the bio-environment.[20–25] Therefore, it is urgent for us to develop some rapid steps to determine, enrich and remove Hg^{2+} on-site. An enormous number of methods have been developed for Hg^{2+} detection or separation in practice. However, most of the existing reports are limited to detecting or separating Hg^{2+} alone. Moroever, most of them cannot be utilized reversibly, which would result in severe secondary pollution.

It is well known that gold nanoparticles (AuNP) exhibit special affinity to mercury by virtue of the fact that mercury could be absorbed onto AuNP to form a gold amalgam.[24,26–29] A series of AuNP-based sensors have been developed for the determination and separation of Hg^{2+}.[23,25,30–34] For example, using unmodified gold nanoparticles as indicators, Memon *et al.*[35] developed a method for Hg^{2+} colorimetric detection, which provided in-depth insight into the rational design of mercury-specific oligonucleotides sensors. Our group[36] also developed an environment-friendly graphene–AuNP composite for the "naked-eye" detection, enrichment, and separation of Hg^{2+} by virtue of the high specific area of the graphene scaffolds and the synergistic interaction between graphene and AuNP. However, the expensive graphene matrix was quite difficult to produce and high specific area would result in the easy aggregation of graphene–AuNP, which could not be applied widely and conveniently in practice.[37–39] Therefore, improving the performance-price ratio by optimizing the structure of the sensing materials remains a huge challenge for their future application.

With this aim in mind, in this study, chitosan–AuNP composite and its functionalized paper strips were designed and developed for sensing and removing Hg^{2+} in aqueous environment. By virtue of the dual supporting roles of the chitosan and the filter paper, AuNP chromophores could be well dispersed either in solution or in the solid state. This sensor is expected to selectively and reversibly recognize Hg^{2+} with a visible colour change based on the special interaction between

School of Chemistry and Chemical Engineering, Qufu Normal University, Qufu, 273165, China. E-mail: yanzhq2008@163.com

gold and mercury. To the best of our knowledge, this is the first report for the environment-friendly sensing and removal of Hg^{2+} based on common paper-based sensors.

2. Experimental

2.1 Reagents and apparatus

Gold(III) chloride trihydrate, chitosan, mercury(II) nitrate, ascorbic acid and all the other chemicals were of analytical grade and purchased from Shanghai Chemical Reagent Company, and used without any purification. Water used was doubly deionized. A series of mouse fibroblast cells (L929) were obtained from Institute of Biochemistry and Cell Biology (the Chinese academy of Sciences, Shanghai, China).

Phosphate buffers were prepared by mixing 0.001 mol L^{-1} H_3PO_4, 0.001 mol L^{-1} K_2HPO_4, 0.001 mol L^{-1} KH_2PO_4 or 0.001 mol L^{-1} KOH aqueous solution in a proper ratio to obtain the desired pH (pH = 3.0, 4.0, 4.5, 5.0, 5.5, 6.0, 7.0, 8.0).

The as-prepared chitosan–AuNPs were characterized *via* transmission electron microscopy (TEM) using a JEOL JEM-2100F TEM (operated at 200 kV). FT-IR spectra were recorded using samples as KBr pellets on a PerkinElmer Model 882 infrared spectrometer scanning from 4000–500 cm^{-1}. Hg^{2+} concentration in the filtrate was determined using an inductively coupled plasma mass spectrometer (PerkinElmer, Elan DRC Plus). UV-vis spectra were recorded on a Lambda 35 UV/Vis spectrometer (PerkinElmer Precisely) using a 1 cm^2 quartz cell. pH was measured using a PHS-25 pH meter.

2.2 Preparation of chitosan–AuNP

Into a 100 mL round-bottom flask, 0.375 g (0.025 mol) chitosan, 35.0 mL doubly deionized water and 0.7 mL glacial acetic acid were added and maintained at 55 °C for 5.0 h. To the mixture, 3.0 mL 10.0 g L^{-1} gold(III) chloride trihydrate solution was added, and the mixture was further stirred for 45 min. After the temperature was increased to 85 °C, 0.75 mL 0.1 mol L^{-1} ascorbic acid was added to reduce gold(III) chloride trihydrate to nanogold, resulting in the color change to dark red. After maintaining the temperature for another 20 min, the resulting composite was cooled to room temperature, centrifuged and washed with enough deionized water, and then dried under vacuum at 50 °C to obtain dark red chitosan–AuNP.

2.3 Preparation of paper strips functionalized by chitosan–AuNPs

A common filter paper with a diameter of 7.0 cm (No: GB/T1914-2007) was immersed overnight in a chitosan–AuNP dispersion in water (3.5×10^{-3} g L^{-1}, pH 5.0 and $c_{\text{ascorbic acid}} = 1.0 \times 10^{-4}$ mol L^{-1}), and then dried under vacuum.[40–42] The resulting filter paper functionalized with chitosan–AuNP chromophore was then cut into the shape needed for colorimetric detection or removal of Hg^{2+}.

2.4 Preparation of environmental water samples

Three different environmental water samples were taken randomly from the Yi River, underground water and tap water on campus, which were further filtered several times and concentrated by 100 times using the N_2 blowing methods. The as-prepared samples were stored at room temperature for subsequent analyses.

2.5 Preparation of fruit or vegetable samples

Fresh fruits or vegetables were all purchased from the local farm produce market near Qufu Normal University, China. After all the fruits or vegetables were washed and dried in the air, the edible parts were cut into 0.5 cm^3 and blended using a juice extractor. Next, 20 mL suspensions of each were taken and then, they were further centrifuged at 5000 rpm for 20 min. The as-prepared fruit or vegetable samples were stored at 4 °C for direct UV-vis spectral or colorimetric analyses.

2.6 Cytotoxicity analysis

Cytotoxicity of the present chitosan–AuNP was estimated by 3-(4,5-dimethyl-2-thiazolyl)-2,5-diphenyl-2*H*-tetrazolium bromide assay (5 mg mL^{-1} MTT in PBS). To perform this assay, a series of mouse fibroblast cell lines (L929) were seeded into 96-well microculture plates (6×10^4 cells per mL, 100 μL per well) for 24 h. Subsequently, the medium (5 mg mL^{-1} MTT in PBS) was changed into chitosan–AuNP solution with different concentrations from 0 to 10^{-3} g L^{-1} and cultured for another 48 h. After treatment, the cytotoxicity of chitosan–AuNP was obtained using a microplate reader by comparing the number of viable cells treated with chitosan–AuNP against those untreated (BioTek, Power Wave XS).

2.7 Hg^{2+} detection procedure

For testing the paper-based sensor, a paper strip functionalized by chitosan–AuNP was immersed into an Hg^{2+} sample solution for 5 min in a closed vial under ambient condition. After it was taken out, the color of the paper strip was recorded and compared with the color of the strip before immersion.

For UV-vis spectral determination, into a 10 mL volumetric flask, 1.0 mL 3.5×10^{-3} g L^{-1} chitosan–AuNP, 1.0 mL pH 5.0 buffer, 1.0 mL 1.0×10^{-4} mol L^{-1} ascorbic acid and 1.0 mL Hg^{2+} sample of different concentrations were transferred. The mixture was then diluted to 10 mL with doubly deionized water and vibrated thoroughly. After incubation for 5.0 min, UV-vis spectra were recorded from 300 nm to 700 nm, and the inverse of the absorption intensity (1/*A*) at 521 nm was used for Hg^{2+} quantitative analyses.

3. Results and discussion

3.1 Optimized fabrication and characterization

To make sure that AuNPs could be grafted tightly and evenly onto the surface of chitosan, the mixture of chitosan gel and $HAuCl_4$ was continuously stirred for 45 min at room temperature before the reaction temperature was maintained at 85 °C

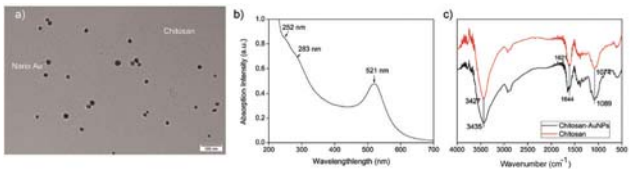

Fig. 1 (a) TEM image; (b) UV-vis spectrum and (c) FTIR spectra of the resultant chitosan–AuNPs.

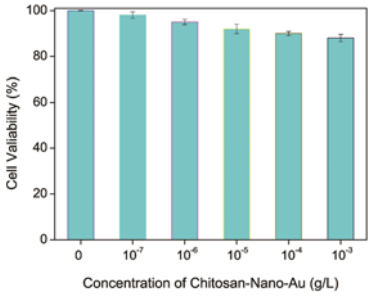

Fig. 2 The cytotoxicity of chitosan–AuNP to a series of mammalian cell lines of L929.

upon the addition of ascorbic acid. It is expected that the electrostatic interaction can occur between the empty d-orbits in the Au atoms and the lone-pair electrons in the O or N atoms before $HAuCl_4$ is reduced to gold nanoparticles.

The as-prepared chitosan–AuNP was characterized by transmission electron microscopy (TEM), and FTIR and UV-vis absorption spectroscopy, as shown in Fig. 1. From the TEM image (Fig. 1a), we find that the resultant AuNP chromophores were uniformly distributed onto the surface of chitosan, with an average diameter of *ca.* 15 nm. The reason may be attributed to the strong chelating interaction between the empty d-orbits in the AuNPs and the lone-pair electrons of the O or N atoms in chitosan, as expected. In the UV-vis spectrum, there is a distinct absorption peak at 521 nm, accompanied by two shoulder peaks at 252 nm and 283 nm (Fig. 1b). The peak at 521 nm originates from the surface plasmon of the AuNPs[36] and the peaks at 252 nm and 283 nm result from the $n \rightarrow \pi^*$ transition of O–H, N–H and C═O bonds in chitosan main chains. All the characterized UV-vis peaks suggest that the as-prepared composite is composed of both AuNP and chitosan. Furthermore, from the FTIR spectra shown in Fig. 1c, we find that the characteristic peaks of pure chitosan are centered at *ca.* 3427, 1621 and 1074 cm^{-1}, ascribed to the stretching vibration of N(O)–H, C–N and C–O bonds, respectively. In the FTIR spectrum of the as prepared chitosan–AuNP composite, all the three characterized peaks shift to longer wavenumbers, *i.e.*, from 3427 to 3435 cm^{-1} for the N(O)–H bond, 1621 to 1644 cm^{-1} for the C–N bond and 1074 to 1089 cm^{-1} for the C–O bond. The shift in the FTIR peaks to higher wavenumbers further confirm that AuNPs graft on the surface of the chitosan *via* electrostatic interactions between the empty d-orbit of the Au atom and the lone-pair electron in O atom or N atom, resulting in increased electronegativity of the N or O atoms on coordinating with the electron-deficient Au atoms.

3.2 Cytotoxicity of chitosan–AuNP

To evaluate the environment-friendly nature of the as-prepared chitosan–AuNP, its cytotoxicity towards a series of mouse fibroblast cell lines (L929) was measured and the results are shown in Fig. 2. From Fig. 2, we could find that more than 88% cells are still kept viable in the tested cell line after they have been exposed to the chitosan–AuNP medium even at the highest concentration of 10^{-3} g L^{-1} for 48 h. Accordingly, the as-prepared chitosan–AuNP composite expresses quite low toxicity to mammalian cells at the concentrations applied for colorimetric sensing of Hg^{2+} in environmental samples.

3.3 Enrichment and removal ability of Hg^{2+} by chitosan–AuNP

To illustrate the removal ability of Hg^{2+} by the as-prepared chitosan–AuNP composite, the content of Hg^{2+} in some given aqueous samples before and after treating with the as-prepared chitosan–AuNP functionalized filter-paper were measured by inductively coupled plasma spectrometry (ICP). For this experiment, 50.0 mL aqueous samples with different Hg^{2+} concentrations (1.0×10^{-5}, 5.0×10^{-6} and 1.0×10^{-6} mol L^{-1}) were filtered repeatedly for 3 times through the chitosan–AuNP functionalized filter-paper. The Hg^{2+} content remaining in the resultant filtrates were measured repeatedly for 5 times. The results are shown in Table 1. More than 93.5% Hg^{2+} in the aqueous samples could be absorbed and removed by the as-prepared chitosan–AuNP-functionalized filter-paper, with an initial Hg^{2+} concentration as high as 1.0×10^{-5} mol L^{-1}, suggesting that the resultant chitosan–AuNP functionalized filter paper, as a stationary phase, will be potentially useful for the enhanced removal Hg^{2+} in aqueous media.

3.4 The action mechanism between chitosan–AuNP and Hg^{2+}

To experimentally confirm the action mechanism of chitosan–AuNP to absorb Hg^{2+}, TEM images with elemental analysis and high-resolution TEM were performed to illustrate the chemical composition of the present chitosan–AuNP in the absence or presence of Hg^{2+} (Fig. 3). From Fig. 3, we find that after reaction with Hg^{2+}, the resultant gold amalgam nanoparticles are slightly larger than the original chitosan–AuNP. This might result from the reaction between chitosan–AuNP and Hg^{2+} to form a new layer of gold amalgam onto the chitosan–AuNP in the presence of ascorbic acid.[43,44] The corresponding elemental analysis intuitively confirms that no mercury is found in the original chitosan–AuNP (Fig. 3c),

Table 1 Hg^{2+} removal ability for chitosan–AuNP-functionalized filter-paper (n = 5)

$c_{Hg^{2+}}$ Spiked in sample (10^{-8} M)	$c_{Hg^{2+}}$ found in the filtrate (10^{-8} M)	Hg^{2+} absorption efficiency (%)	Relative standard deviation (%)
1000	65	93.5	3.7
500	30	94.0	2.5
100	4.8	95.2	4.4

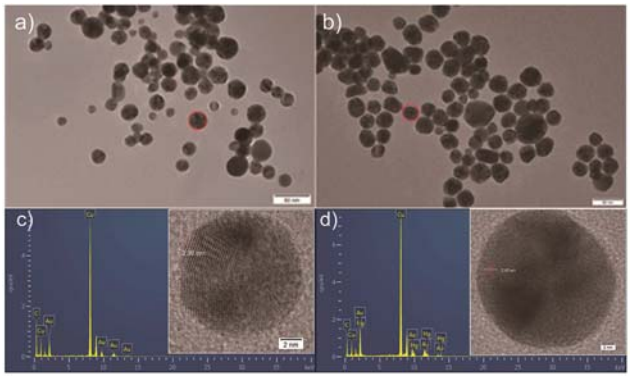

Fig. 3 TEM images of chitosan–AuNP (a) before and (b) after interaction with Hg^{2+}; elemental analyses of the resultant nanoparticles (c) before and (d) after reaction with Hg^{2+} and their corresponding high-resolution TEM images (Inserts in c and d).

while both Au and Hg emerge after chitosan–AuNP reacts with Hg^{2+} (Fig. 3d). Furthermore, from the high-resolution TEM images (insets in Fig. 3c), we find that the fringe spacing was 0.238 nm in the pure gold nanoparticle, which well matches the [111] interplanar spacing of nanogold.[36] Moreover, the lattice fringe spacing enlarges to 0.245 nm upon addition of Hg^{2+} in the presence of ascorbic acid (insert in Fig. 3d), hinting that Hg^{2+} is reduced to elemental mercury, which further diffuses onto the AuNP to form a highly defective gold amalgam. The action mechanism between chitosan–AuNP and Hg^{2+} in the presence of ascorbic acid is accordingly proposed to form a gold amalgam, in accordance with previous literature reports.[36,45,46]

3.5 Application for visually sensing trace Hg^{2+}

3.5.1. Optimization of analytic conditions. It is well known that pH will have a large effect on the redox potential. The effect of pH over 3.0–8.0 was investigated first. As shown in Fig. 4, it is easy to observe that the absorption intensity of the chitosan–AuNP aqueous dispersion at 521 nm remains nearly unchanged in the entire tested pH range, suggesting that the present chitosan–AuNP is quite stable in the acidic or weakly basic media. Upon addition of Hg^{2+} in the presence of ascorbic acid, the absorption intensity at 521 nm decreases gradually with the decrease in pH, and reaches a minimal platform when pH is *ca.* 5.5. This may result from the fact that the redox potential of Hg^{2+} decreases with the increase in pH. Moreover, the higher OH^- concentration makes the solubility of Hg^{2+} lower in aqueous solution. These two reasons will result in less Hg^{2+} to be reduced accompanying along with weaker response. Accordingly, pH 5.0 was selected for all the subsequent experiments.

To express the response rate and stability of the proposed chitosan–AuNP to heavy metal Hg^{2+}, the absorption intensity at 521 nm was recorded from 0 to 1.0 h after addition of Hg^{2+} in the presence of ascorbic acid. From Fig. 5, we observe a fast response of less than 5.0 min for the proposed chitosan–AuNP towards Hg^{2+}, which remains unchanged over the following 1 h. Furthermore, the effect of ionic strength on the absorption peak at 521 nm was investigated by changing the NaCl concentration from 2.0×10^{-2} mol L^{-1} to 1.0×10^{-7} mol L^{-1}. No distinct change takes place, hinting that the proposed chitosan–AuNP is stable for application in various complicated environments.

3.5.2. Special selectivity towards Hg^{2+}. To illustrate the sensing selectivity of the proposed chitosan–AuNP towards Hg^{2+}, its UV-vis spectra from 300 nm to 700 nm were recorded in the presence of some environmentally relevant metal ions as their nitrate salts, namely, Al^{3+}, Ba^{2+}, K^+, Mg^{2+}, Na^+, Ni^{2+}, Pb^{2+}, Sr^{2+}, Cd^{2+}, Co^{3+}, Cu^{2+}, Fe^{3+} and Ag^+ in 2.0×10^{-4} mol L^{-1}, except for Hg^{2+} in 2.0×10^{-6} mol L^{-1}. As shown in Fig. 6, the absorption intensity at 521 nm shows negligible changes upon addition of all the metal ions except Hg^{2+}, which is less than 5% compared with that in the presence of Hg^{2+} even at a 1/100 concentration. In addition, Hg^{2+} could exclusively change the color of the proposed chitosan–AuNP dispersion and its functionalized paper strips from dark-red to yellow (Fig. 6b), suggesting that the proposed chitosan–AuNP system either in solution or as a solid possesses excellent selectivity for the colorimetric sensing of Hg^{2+}.

3.5.3. Analytical parameters and sample analyses. To disclose the rule for chitosan–AuNP to sense Hg^{2+}, UV-vis spectral titration experiments have been performed with different concentrations from 0 to 200.0×10^{-8} mol L^{-1}. The obtained titra-

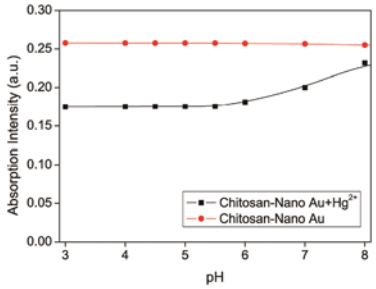

Fig. 4 The effect of pH on the absorption intensity in the presence of the chitosan–AuNP system at 521 nm in the absence or presence of Hg^{2+} ($c_{chitosan-AuNP}$ = 3.5×10^{-4} g L^{-1}, $c_{Hg^{2+}}$ = 2.0×10^{-6} mol L^{-1}, $c_{ascorbic\ acid}$ = 1.0×10^{-5} mol L^{-1}).

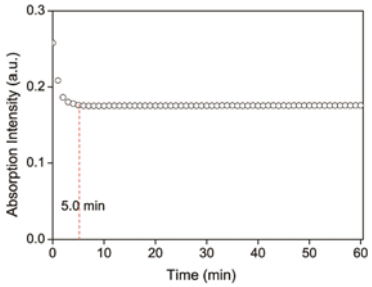

Fig. 5 Time response curve of the proposed chitosan–AuNP system at 521 nm to Hg^{2+} in the presence of ascorbic acid ($c_{chitosan-AuNP}$ = 3.5×10^{-4} g L^{-1}, $c_{Hg^{2+}}$ = 2.0×10^{-6} mol L^{-1}, $c_{ascorbic\ acid}$ = 1.0×10^{-5} mol L^{-1}, pH = 5.0).

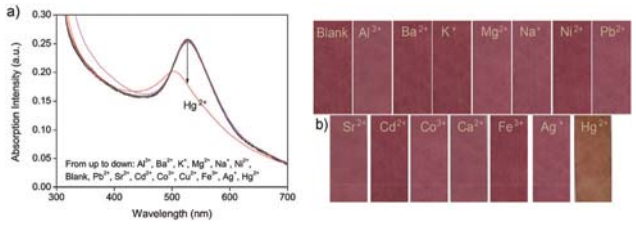

Fig. 6 The selectivity of the proposed chitosan–AuNP system to different metal ions by (a) UV-vis spectra (from top to bottom: Al^{3+}, Ba^{2+}, K^{+}, Mg^{2+}, Na^{+}, Ni^{2+}, blank, Pb^{2+}, Sr^{2+}, Cd^{2+}, Co^{3+}, Cu^{2+}, Fe^{3+}, Ag^{+} and Hg^{2+}); (b) the color change of chitosan–AuNP functionalized paper-strips ($c_{\text{chitosan–AuNP}}$ = 3.5 × 10^{-4} g L^{-1}, $c_{\text{ascorbic acid}}$ = 1.0 × 10^{-5} mol L^{-1}, pH = 5.0).

tion results accompanied by the visual color change are shown in Fig. 7. From Fig. 7, some key analysis parameters, namely, the calibration graph, detection limit and precision could be obtained under optimized conditions. A linear relationship between 1/*A* at 521 nm and $c_{Hg^{2+}}$ is exhibited over the range of 5.0 to 200.0 × 10^{-8} mol L^{-1} with a correlation coefficient of 0.9926. The regression equation is $1/A = -3.9212 + 9.08 \times 10^{-3}\, c$ (10^{-8} mol L^{-1}). Based on the definition of the detection limit (LOD),[47,48] the LOD for sensing Hg^{2+} was determined to be up to 3.2 × 10^{-9} mol L^{-1} by spectral analysis (Fig. 7b) and 5.0 × 10^{-8} mol L^{-1} by paper-based visible colorimetric analysis (Fig. 7c and d). Both of the obtained LODs could meet the requirement for detecting Hg^{2+} in drinking water, as defined by the WHO.[49]

Furthermore, the proposed chitosan–AuNP sensing system was used to detect Hg^{2+} in 3 real environmental water samples (from the Yi River, underground water and tap water in campus) and 4 fruit-vegetable samples (Table 2). For the recovery study, a known concentration of Hg^{2+} (100.0 × 10^{-8} mol L^{-1}) was added and the total Hg^{2+} content was calculated using the proposed method as well as by ICP-MS. As shown in Table 2, the recoveries are between 96.2% and 104.6% with R.S.D. ≤2.6%. Importantly, all the data obtained from the proposed chitosan–AuNPs system agree well with the results either from our reports before using other sensors,[36,46] or the results obtained from inductively coupled plasma mass spectrometry (ICP-MS), validating the reliability and practicality of the proposed methods.

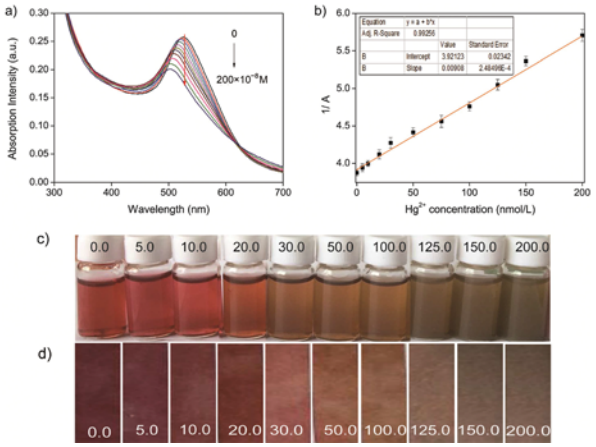

Fig. 7 (a) Absorption spectra of the proposed chitosan–AuNP system in the presence of different $c_{Hg^{2+}}$ (from top to bottom: 0, 5.0, 10.0, 20.0, 30.0, 50.0, 75.0, 100.0, 125.0, 150.0, and 200.0 × 10^{-8} mol L^{-1}); (b) a linear relationship between 1/*A* at 521 nm and $c_{Hg^{2+}}$; the corresponding color change of (c) chitosan–AuNP aqueous solution and (d) its functionalized paper-strips ($c_{\text{chitosan–AuNP}}$ = 3.5 × 10^{-4} g L^{-1}, $c_{\text{ascorbic acid}}$ = 1.0 × 10^{-5} mol L^{-1}, pH = 5.0).

3.6 Reusability of chitosan–AuNP for Hg^{2+} sensing

To make the best utilization of the proposed chitosan–AuNP sensing system, its reusability was studied in detail (Fig. 8). For the chitosan–AuNP aqueous solution, upon addition of Hg^{2+}, a color change from dark-red to yellow (Fig. 8a) was observed due to the formation of gold amalgam onto AuNP. By

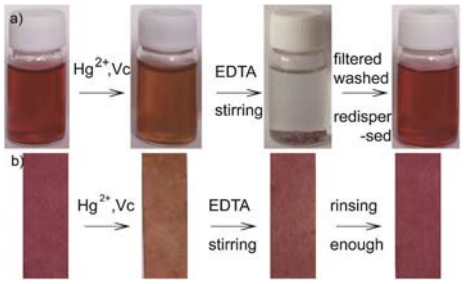

Fig. 8 The reversibility of (a) chitosan–AuNP solution and (b) its functionalized paper-strips.

Table 2 Hg^{2+} sensing results for some real environmental samples (*n* = 5)

Samples	$c_{Hg^{2+}}$ in sample (10^{-8} M)	Spiked (10^{-8} M)	Found (10^{-8} M)	Recovery (%)	R.S.D. (%)	$c_{Hg^{2+}}$ by ICP-MS
The Yi river	39.4[b]	100.0	136.6	98.2	1.6	136.9
Under-ground	76.1[b]	100.0	184.7	104.6	3.3	185.2
Pure water	0.00[b]	100.0	96.2	96.2	0.9	95.9
Asparagus lettuce	0.00	100.0	103.5	103.5	2.6	100.6
Spinacia oleracea	0.00	100.0	97.1	97.1	1.7	99.7
Dang-shan pear	0.00	100.0	99.4	99.4	1.6	100.8
Red apple	0.00	100.0	104.2	104.2	3.1	100.2

[a] Phosphate buffer, pH 5.0. [b] The real values are the table values ×10^{-2} for the detected water samples concentrated by 100 times using N_2 blowing methods.

virtue of the strong coordination between ethylenediaminetetraacetic acid (EDTA) and Hg^{2+}, addition of a sufficient amount of EDTA into the mixture under vigorous overnight stirring in oxygen atmosphere results in a colorful sediment. Chitosan–AuNP is accordingly regenerated by extracting mercury from the resulting Au–Hg assembly. After the colorful sediment is filtered and washed with enough water, it could be re-dispersed to regenerate a dark-red uniform dispersion by sonication, possessing the same UV-vis spectrum shown in Fig. 1b. The proposed chitosan–AuNP functionalized paper strips could also be regenerated after reacting with a sufficient amount of EDTA and rinsing with pure water several times (Fig. 8b). The above results suggest that the proposed chitosan–AuNP sensing systems can be repeatedly regenerated and utilized.

4. Conclusions

An environment-friendly chitosan–Au nanocomposite (chitosan–AuNP) and its functional paper strips have been identified and developed for the reversible colorimetric sensing and removal of Hg^{2+}, accompanied by a visible color change from dark-red to yellow. By virtue of the high affinity between nanogold and mercury to form a gold amalgam, the proposed chitosan–AuNP and its functionalized paper strip could enrich and remove more than 93.5% of Hg^{2+} in an aqueous solution with an initial concentration as high as 1.0×10^{-5} mol L^{-1} by a simple filtration process. Both the chitosan–AuNP dispersion and its functionalized paper strips are efficiently applied as reusable colorimetric sensors to recognize Hg^{2+} in real aqueous and some fruit or vegetable juice samples with excellent recoveries between 96.2% and 104.6% and a low R.S.D. of $\leq$2.6%. Owing to their low toxicity, the proposed chitosan–AuNP sensing systems would provide general and effective insight for constructing environment-friendly composites for the sensing and removal of various toxic materials without sophisticated instruments.

Conflicts of interest

Q10 ■■■■

Acknowledgements

The authors gratefully acknowledge the financial supports from Shandong Provincial Natural Science Foundation (No: ZR2018MB038, ZR2016BQ13) and National Natural Science Foundation of China (No: 21806089, 21277103).

Notes and references

1 W. W. He, L. Luo, Q. Y. Liu and Z. B. Chen, *Anal. Chem.*, 2018, **90**, 4770–4775.
2 A. Anwar, A. Minhaz, N. A. Khan, K. Kalantari, A. B. M. Afifi and M. R. Shah, *Sens. Actuators, B*, 2018, **257**, 875–881.
3 J. H. Yang, Y. Zhang, L. Zhang, H. L. Wang, J. F. Nie, Z. X. Qin, J. Li and W. C. Xiao, *Chem. Commun.*, 2017, **53**, 7477–7480.
4 B. K. Momidi, V. Tekuri and D. R. Trivedi, *Spectrochim. Acta, Part A*, 2017, **180**, 175–182.
5 N. A. Azmi and S. C. Low, *J. Water Process Eng.*, 2017, **15**, 37–42.
6 L. L. Tan, Z. B. Chen, Y. Zhao, X. C. Wei, Y. H. Li, C. Zhang, X. L. Wei and X. C. Hu, *Biosens. Bioelectron.*, 2016, **85**, 414–421.
7 L. Y. Bai, L. J. Tou, Q. Gao, P. Bose and Y. L. Zhao, *Chem. Commun.*, 2016, **52**, 13691–13694.
8 Y. S. Guang, X. Ren, S. Zhao, Q. Z. Yan, G. Zhao and Y. H. Xu, *J. Environ. Sci. Health, Part A: Toxic/Hazard. Subst. Environ. Eng.*, 2018, **53**, 555–560. Q11
9 S. Y. Guang, G. Wei, Z. Q. Yan, Y. H. Zhang, G. Zhao, R. L. Wu and H. Y. Xu, *Analyst*, 2018, **143**, 449–457.
10 Z. Q. Yan, Q. Zhao, M. J. Wen, L. Hu, X. Z. Zhang and J. M. You, *Spectrochim. Acta, Part A*, 2017, **186**, 17–22.
11 N. B. Lin, L. W. Cao, Q. L. Huang, C. Y. Wang, Y. Wang, J. Zhou and X. Y. Liu, *Adv. Funct. Mater.*, 2016, **26**, 8885–8902.
12 L. Q. Kong, L. Zhang, Z. H. Meng, C. Xu, N. B. Lin and X. Y. Liu, *Nanotechnology*, 2018, **29**, 315203.
13 S. Y. Guang, J. C. Tian, G. We, Z. Q. Yan, H. F. Pan, J. H. Feng and H. Y. Xu, *Talanta*, 2017, **170**, 89–96.
14 Z. Q. Yan, M. F. Yuen, L. Hu, P. Sun and C. S. Lee, *RSC Adv.*, 2014, **4**, 48373–48388.
15 Z. Q. Yan, S. Y. Guang, H. Y. Xu and X. Y. Liu, *Analyst*, 2011, **136**, 1916–1921.
16 Z. L. Qiu, J. Shu, G. X. Jin, M. D. Xu, Q. H. Wei, G. N. Chen and D. P. Tang, *Biosens. Bioelectron.*, 2016, **77**, 681–686.
17 J. F. Chen, J. Tang, J. Zhou, L. Zhang, G. N. Chen and D. P. Tang, *Anal. Chim. Acta*, 2014, **810**, 10–16.
18 J. Y. Zhuang, L. B. Fu, D. P. Tang, M. D. Xu, G. N. Chen and H. H. Yang, *Biosens. Bioelectron.*, 2013, **39**, 315–319.
19 Y. Song, Z. F. Lin, L. Q. Kong, Y. Xing, N. B. Lin, Z. S. Zhang, B. H. Chen and X. Y. Liu, *Adv. Funct. Mater.*, 2017, **27**, 1700628.
20 S. K. Kim, M. Gupta and H. I. Lee, *Sens. Actuators, B*, 2018, **257**, 728–733.
21 R. Ayranci, D. O. Demirkol, S. Timur and M. Ak, *Analyst*, 2017, **142**, 3407–3415.
22 R. Sedghi, S. Kazemi and B. Heidari, *Sens. Actuators, B*, 2017, **245**, 860–867.
23 F. Zarlaida and M. Adlim, *Microchim. Acta*, 2017, **184**, 45–58.
24 Z. B. Chen, C. M. Zhang, Q. G. Gao, G. Wang, L. L. Tan and Q. Liao, *Anal. Chem.*, 2015, **87**, 10963–10968.
25 Q. Wang, X. H. Yang, X. H. Yang, P. Liu, K. M. Wang, J. Huang, J. B. Liu, C. X. Song and J. J. Wang, *Spectrochim. Acta, Part A*, 2015, **136**, 283–287.
26 Z. J. Barton and J. Rodriguez-Lopez, *Anal. Chem.*, 2014, **86**, 10660–10667.

27 Z. Guo, G. Q. Chen, G. M. Zeng, Z. W. Li, A. W. Chen, M. Yan, L. Z. Liu and D. Y. Huang, *RSC Adv.*, 2014, **4**, 59275–59283.

28 Z. Q. Yan, L. Hu and J. M. You, *Anal. Methods*, 2016, **8**, 5738–5754.

29 S. Z. Lv, K. Y. Zhang, Y. Y. Zeng and D. P. Tang, *Anal. Chem.*, 2018, **90**, 7086–7093.

30 X. J. Liu, Z. J. Wu, Q. Q. Zhang, W. F. Zhao, C. H. Zong and H. W. Gai, *Anal. Chem.*, 2016, **88**, 2119–2124.

31 J. J. Du, Z. K. Wang, J. L. Fan and X. J. Peng, *Sens. Actuators, B*, 2015, **212**, 481–486.

32 J. J. Du, S. Y. Yin, L. Jiang, B. Ma and X. D. Chen, *Chem. Commun.*, 2013, **49**, 4196–4198.

33 L. H. Wang, Y. Zeng, A. G. Shen, Y. C. Fu, L. W. Zeng and J. M. Hu, *RSC Adv.*, 2016, **6**, 86025–86033.

34 Y. Zeng, L. H. Wang, L. W. Zeng, A. G. Shen and J. M. Hu, *Talanta*, 2017, **162**, 374–379.

35 A. G. Memon, X. H. Zhou, J. C. Liu, R. Y. Wang, L. H. Liu, B. F. Yu, M. He and H. C. Shi, *J. Hazard. Mater.*, 2017, **321**, 417–423.

36 Z. Q. Yan, H. T. Xue, K. Berning, Y. W. Lam and C. S. Lee, *ACS Appl. Mater. Interfaces*, 2014, **6**, 22761–22768.

37 Z. Q. Yan, W. L. Yao, L. Hu, D. D. Liu, C. D. Wang and C. S. Lee, *Nanoscale*, 2015, **7**, 5563–5577.

38 T. N. Anh, A. D. Chowdhury and R. A. Doong, *Sens. Actuators, B*, 2017, **252**, 1169–1178.

39 Z. Y. Yan, X. C. Qu, Q. Q. Niu, C. Q. Tian, C. J. Fan and B. F. Ye, *Anal. Methods*, 2016, **8**, 1565–1571.

40 Z. Q. Yan, X. Z. Zhang, C. Bao, H. Tang, Q. Zhao, L. Hu and J. M. You, *Sens. Actuators, B*, 2018, **262**, 869–875.

41 W. Q. Lai, Q. H. Wei, M. D. Xu, J. Y. Zhuang and D. P. Tang, *Biosens. Bioelectron.*, 2017, **89**, 645–651.

42 Z. L. Qiu, J. Shu and D. P. Tang, *Anal. Chem.*, 2017, **89**, 5152–5160.

43 X. H. Sun, C. P. Li, W. K. Wong, N. B. Wong, C. S. Lee, S. T. Lee and B. K. Teo, *J. Am. Chem. Soc.*, 2002, **124**, 14464–14471.

44 K. A. Abel, J. C. Boyer, C. M. Andrei and F. C. J. M. van Veggel, *J. Phys. Chem. Lett.*, 2011, **2**, 185–189.

45 F. Afzali, M. H. A. Zavar, G. Rounaghi and N. Ashraf, *Electrochim. Acta*, 2016, **209**, 654–660.

46 Z. Q. Yan, L. Hu, L. Nie and J. M. You, *RSC Adv.*, 2016, **6**, 109857–109861.

47 Z. Q. Yan, G. Wei, S. Y. Guang, M. M. Xu, X. Ren, R. L. Wu, G. Zhao, F. Y. Ke and H. Y. Xu, *Dyes Pigm.*, 2018, **159**, 542–550.

48 Z. Q. Yan, L. Hu, L. Nie and J. M. You, *RSC Adv.*, 2016, **6**, 109857–109861.

49 L. B. Zhang, L. Tao, B. L. Li, L. Jing and E. K. Wang, *Chem. Commun.*, 2010, **46**, 1476–1478.